

**Dataset S1:** Landsat ETM+, OLI and Terra-ASTER L1T data used in the present study.

(File uploaded separately as Data\_Set\_S1.xlsx)

**Dataset S2:** GL migration values generated in this study  
(File uploaded separately as Data\_Set\_S2.xlsx)

**Table S1.** Landsat and Terra-ASTER positional uncertainty estimations ( $1\sigma$ ) for MBLS grounded ice boundary classifications (cf. Section 2.1.2.). Values derived following the methodology of Bindshadler et al. (2011) and Christie et al. (2016; see their Text S1).

<i>Platform (Sensor)</i>	<i>Year Mapped</i>	<i>Grounded Ice Boundary Classification</i>	<i>Spatial Resolution (m)</i>	<i>Prescribed Pixel Error (m)</i>	<i>Geometric Error<sup>1</sup> (m)</i>	<i>Positional Error (<math>1\sigma</math>; m)</i>
Landsat 7 (ETM+ <sup>2</sup> )	c. 2003 c.2008 2010	Open ocean		1 (30)		58
		Grounded- ice/Sea-ice	30	2 (60)	$\leq 50$	78
		Slow-ice-to Shelf or Outlet Glacier		3 (90)		103
Landsat 8 (OLI <sup>3</sup> )	2015	Open ocean		1 (30)		32
		Grounded- ice/Sea-ice	30	2 (60)	$\leq 12$	61
		Slow-ice-to Shelf or Outlet Glacier		3 (90)		91
Terra (ASTER <sup>4</sup> )	2003	Open ocean		1 (15)		21
		Grounded- ice/Sea-ice	15	2 (30)	$\leq 15$	34
		Slow-ice-to Shelf or Outlet Glacier		3 (45)		47

<sup>1</sup>Geometric error values derived from Lee et al. (2004); Tucker et al. (2004), Storey et al. (2014) and USGS (2015). <sup>2</sup>Enhanced Thematic Mapper Plus. <sup>3</sup>Operational Land Imager. <sup>4</sup>Advanced Spaceborne Thermal Emission and Reflection Radiometer.

**Table S2.** Between-sensor propagated error estimates (metres), associated with combining ASTER L1T and ETM+ (for mapped years 2003-2008); ETM+ and ETM+ (2003-2008); or ETM+ and OLI (2010-2015) datasets. Values derived following the methodology of Christie et al. (2016; their Text S1). Crossed-out matrix cells indicate n/a.

		Platform (Sensor)		
		Landsat 7 (ETM+)	Landsat 8 (OLI)	Terra (ASTER)
Platform (Sensor)	Landsat 7 (ETM+)	82 <sup>a</sup> 110 <sup>b</sup> 146 <sup>c</sup>	66 <sup>a</sup> 99 <sup>b</sup> 137 <sup>c</sup>	61 <sup>a</sup> 85 <sup>b</sup> 113 <sup>c</sup>
	Landsat 8 (OLI)	66 <sup>a</sup> 99 <sup>b</sup> 137 <sup>c</sup>		
	Terra (ASTER)	61 <sup>a</sup> 85 <sup>b</sup> 113 <sup>c</sup>		

<sup>a</sup>Open Ocean, <sup>b</sup>Grounded-ice/Sea-ice, and <sup>c</sup>Slow-ice-to Shelf or Outlet Glacier error estimates (following the nomenclature of Table S1).

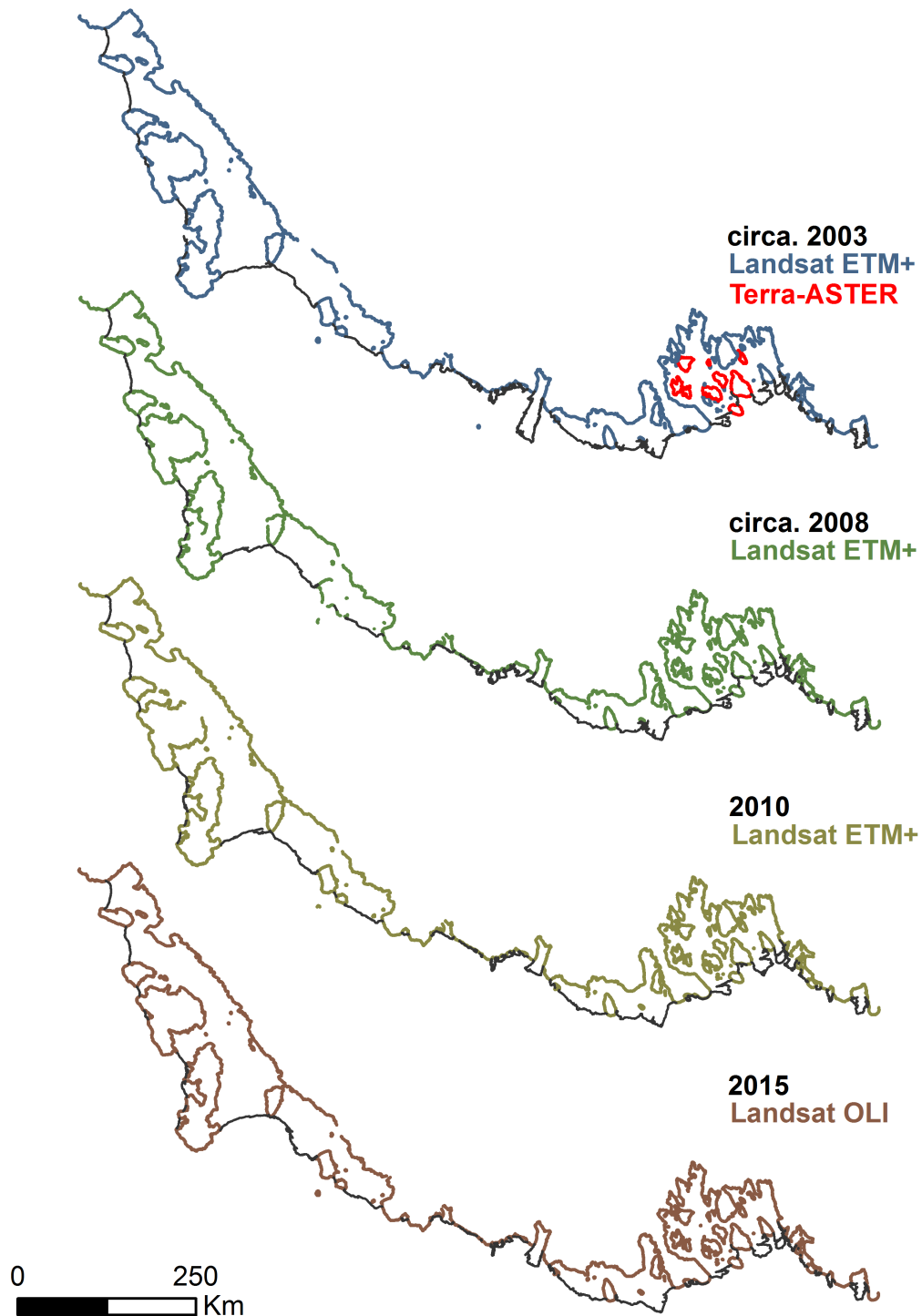


**Figure S1.**  $I_b$  coverage for years circa. 2003, circa. 2008, 2010 and 2015, recovered from Landsat and Terra-ASTER imagery. Thin grey lines denote mean summertime ice-shelf frontal positions, derived as part of the mapping process.

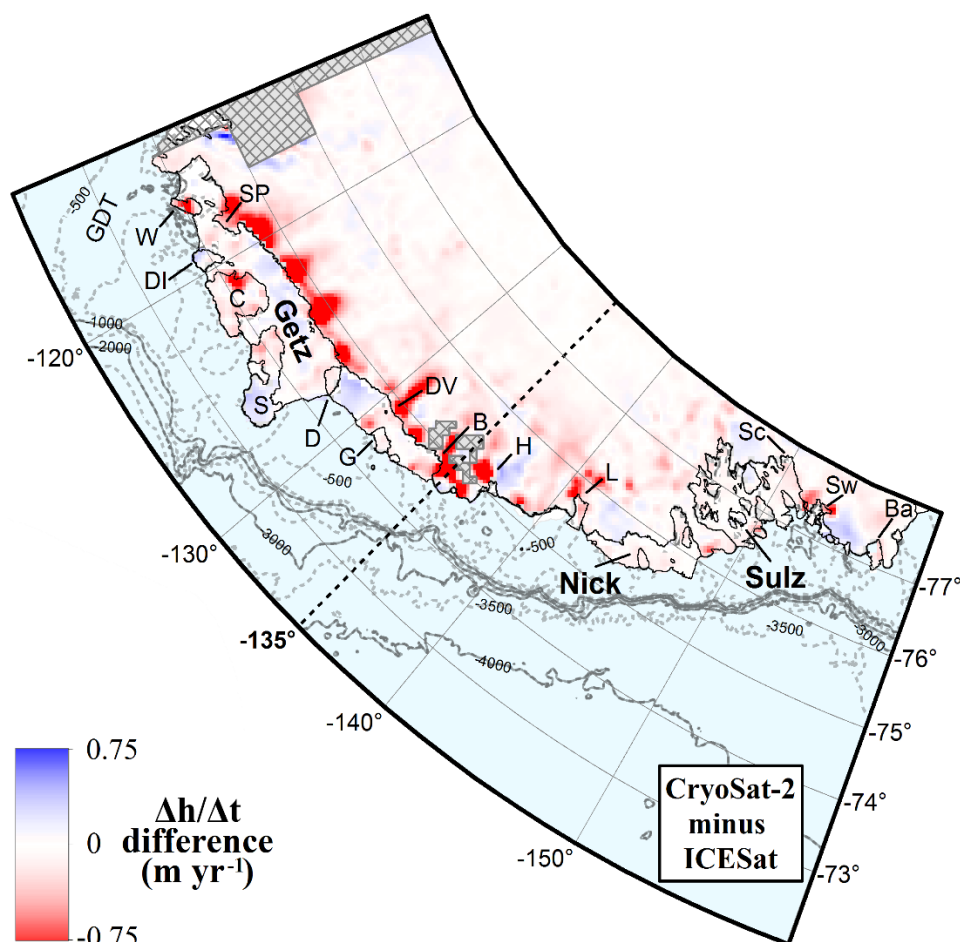


**Figure S2.** Difference in MBLS  $\Delta h/\Delta t$  between the CryoSat-2 and ICESat eras (CryoSat-2 minus ICESat). Negative  $\Delta h/\Delta t$  denotes increased rates of surface elevation change. Artefacts associated with exceptionally steep and/or mountainous terrain upstream of Dotson Ice Shelf (~114-115° W) and near Berry Glacier ('B') are masked (light grey hatching). Site labels and bathymetric contours same as Figure 1 and 2.

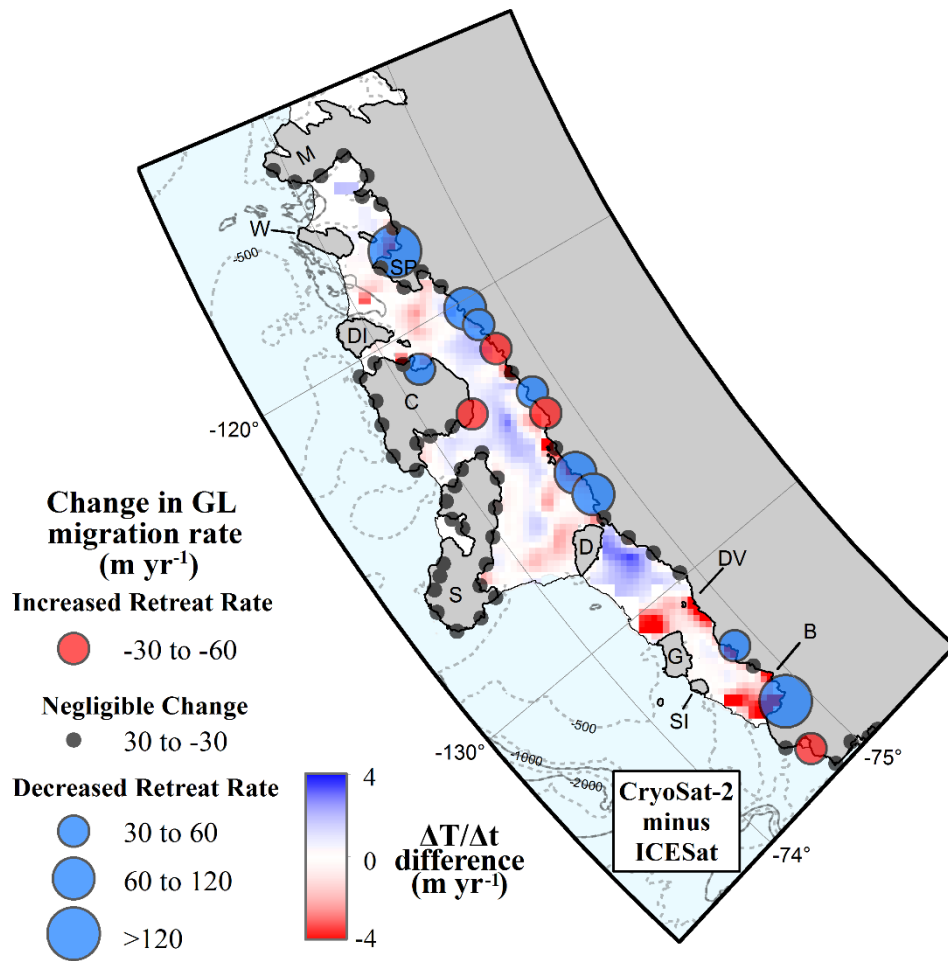


**Figure S3.** Change in Getz Ice Shelf GL migration rate, superimposed over the difference in  $\Delta T/\Delta t$  between the CryoSat-2 and ICESat eras (CryoSat-2 minus ICESat). Positive (blue) GL migration change denotes reduced GL retreat rate. Black circles denote negligible change within satellite error bounds, as per Figures 1, 2 and 3. Positive  $\Delta T/\Delta t$  denotes reduced rates of ice-shelf thinning (implying thickening). Thickness change rates were calculated following the methodology of Pritchard et al. (2012) and Paolo et al. (2015) (see Section 2.2 for further information). Site labels and bathymetric contours as for Figures 3a and 3b.

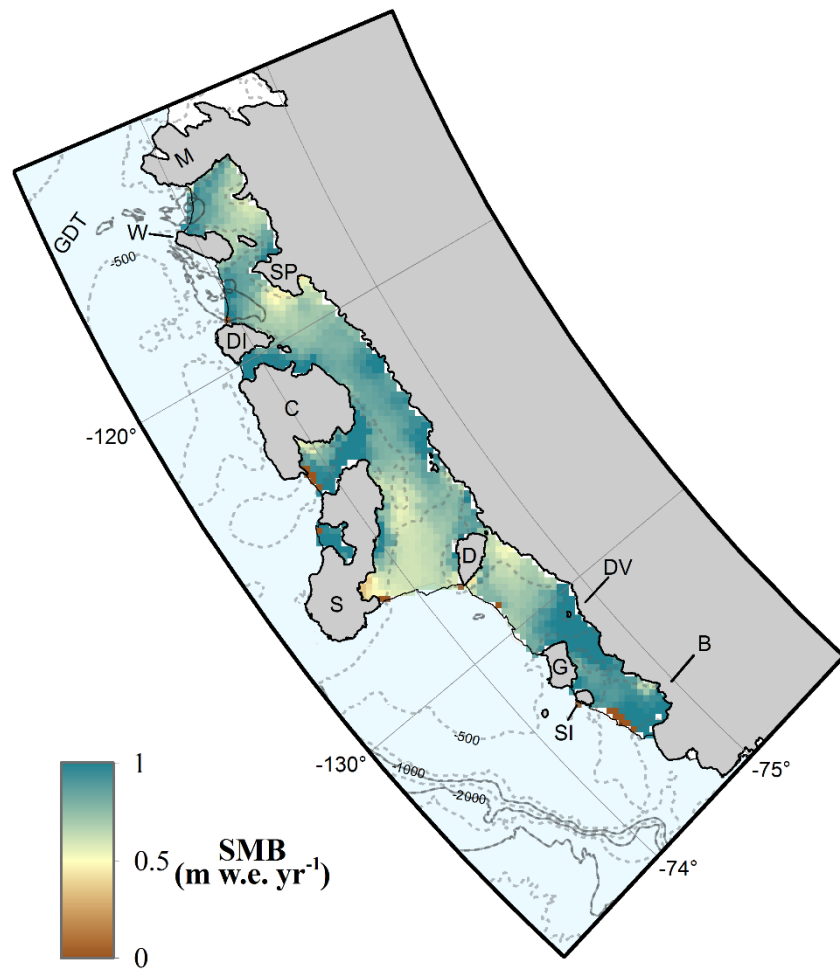


**Figure S4:** 2010-2015 mean surface mass balance (SMB) over Getz Ice Shelf ( $\text{m w.e. yr}^{-1}$ ), derived from RACMO2.3p2 (Lenaerts et al., 2017). Shelf-averaged surface mass balance equals  $0.81 \text{ m w.e. yr}^{-1}$ .



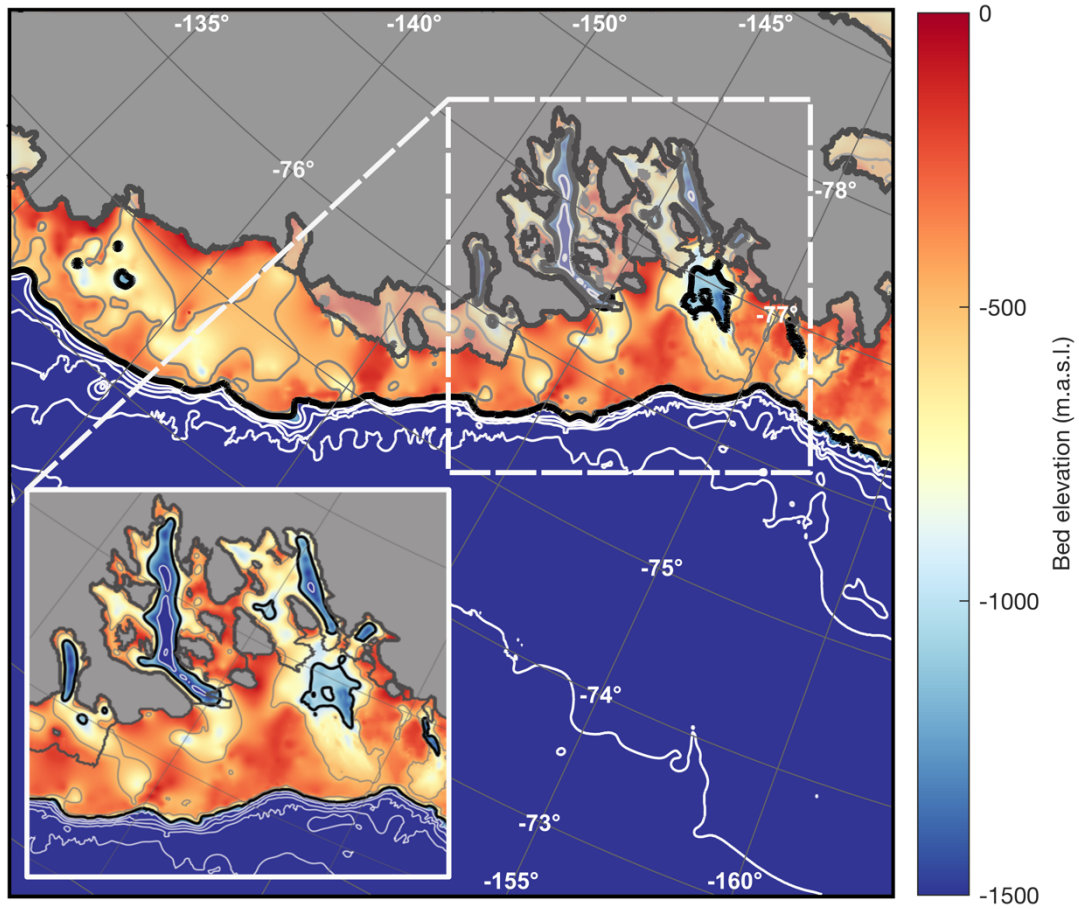


**Figure S5.** Continental shelf morphology along the region west of 135° W (Arndt et al., 2013). Thick black line denotes the 1000 m depth contour, which delineates the approximate location of the continental shelf break and numerous instances of deep, on-shelf bathymetric depressions. White (deep ocean) and light grey (on-continental shelf) lines = 500 m depth increments. Semi-transparent grey patches denote ice shelf spatial limits; grey patches denote fully grounded ice. Inset = continental shelf and sub-ice shelf bathymetry zoomed over the Sulzberger Ice Shelf region. Note the deep subglacial troughs (max. depth 2100 m) which originate within close proximity to the GL near 77/78° S, and which terminate near -but do not bisect- the continental shelf break (see main text for further discussion). In both plots, dark grey lines denote Bedmap 2-derived grounding line and ice-shelf frontal positions (Fretwell et al., 2013). Figure made using Antarctic Mapping Tools (Greene et al., 2017).

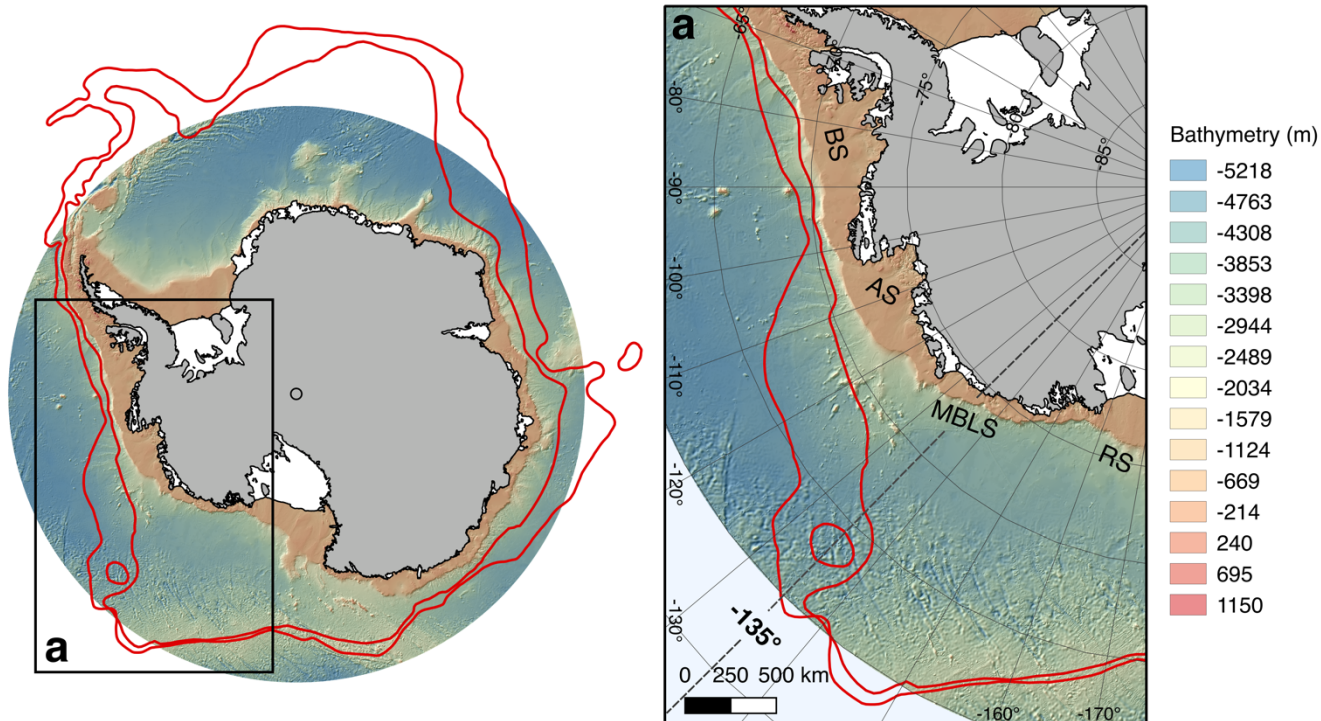


**Figure S6.** Meridional extent of the Antarctic Circumpolar Current (ACC), following Orsi et al. (1995). Red lines denote the Southern Antarctic Circumpolar Current Front (north) and Southern Boundary (south) of the ACC. Data superimposed over IBCSO v.1 circum-Antarctic bathymetry data (Arndt et al., 2013). Inset (a) = ACC position over West Antarctica. Note the proximity of the ACC relative to the shallow continental shelf slopes of the Amundsen (AS) and Bellingshausen (BS) Sea Sectors, as well those offshore from Getz Ice Shelf. Also note the marked northward deflection of the ACC from the continental slope margin at ~130-135° W, which persists to the Ross Sea Sector (RS). See main text for further discussion.

## References for Supplemental Information

- Arndt, J. E., Schenke, H. W., Jakobsson M., Nitsche, F. O., Buys, G., Goleby, B., Rebesco, M., Bohoyo, F., Hong, J., Black, J., Greku, R., Udintsev, G., Barrios, F., Reynoso-Peralta, W., Taisei, M., and Wigley, R.: The International Bathymetric Chart of the Southern Ocean (IBCSO) Version 1.0—A new bathymetric compilation covering circum- Antarctic waters, *Geophys. Res. Lett.*, 40, 3111-3117, doi:10.1002/grl.50413, 2013.
- Christie, F. D. W., Bingham, R. G., Gourmelen, N., Tett, S. F. B., and Muto, A.: Four-decade record of pervasive grounding line retreat along the Bellingshausen margin of West Antarctica, *Geophys. Res. Lett.*, 43, 5741–5749, doi:10.1002/2016GL068972, 2016.
- Fretwell, P., et al.: Bedmap2: Improved ice bed, surface and thickness datasets for Antarctica, *Cryosphere*, 7, 375–393, doi:10.5194/tc-7-375-2013, 2013.
- Greene, C. A., Gwyther, D. E., and Blankenship, D. D.: Antarctic Mapping Tools for MATLAB, *Comput. Geosci.*, 104, 151-157, <https://doi.org/10.1016/j.cageo.2016.08.003>, 2017.
- Lee, D. S., Storey, J. C., Choate, M. J., and Hayes, R. W.: Four Years of Landsat-7 On-Orbit Geometric Calibration and Performance, *IEEE Trans. Geosci. Remote Sens.*, 42(12), 2786-2795, doi:10.1109/TGRS.2004.836769, 2004.
- Orsi, A. H., Whitworth, T. III., And Nowlin Jr, W. D.: On the meridional extent and fronts of the Antarctic Circumpolar Current, *Deep-Sea Res. I*, 42, 64-673.
- Paolo, F. S., Fricker, H. A., and Padman, L.: Volume loss from Antarctic ice shelves is accelerating, *Science*, 348, 327–331, doi:10.1126/science.aaa0940, 2015.
- Pritchard, H. D., Ligtenberg, S. R. M., Fricker, H. A., Vaughan, D. G., van den Broeke, M. R., and Padman, L.: Antarctic ice-sheet loss driven by basal melting of ice-sheets, *Nature*, 484, 502–505, doi:10.1038/nature10968, 2012.
- Storey, J., Choate, M., and Lee, K.: Landsat 8 Operational Land Imager On-Orbit Geometric Calibration and Performance, *Remote Sens.*, 6(11), 11127-11152, doi: 10.3390/rs6111127, 2014.
- Swithinbank, C., Williams, R. S., Jr., Ferrigno, J. G., Foley, K. M., and Rosanova, C. E.: Coastal-change and glaciological map of the Bakutis Coast area, Antarctica: 1972-2002: U.S. Geological Survey Geologic Investigations Series Map, I-2600-F; scale: 1:1,000,000, with accompanying pamphlet (10 p.), 2003a.
- Swithinbank, C., Williams, R. S., Jr., Ferrigno, J. G., Foley, K. M., Hallam, C. A., and Rosanova, C. E.: Coastal-change and glaciological map of the Saunders Coast area, Antarctica: 1972-1997: U.S. Geological Survey Geologic Investigations Series Map, I-2600-G; scale: 1:1,000,000, with accompanying pamphlet (9 p.), 2003b.
- Tucker, C. J., Grant, D. M., and Dykstra, J. D.: NASA's Global Orthorectified Landsat Data Set Compton, *Photogramm. Eng. Remote Sens.*, 70(3), 313-322, doi: 10.14358/PERS.70.3.313, 2004.
- United States Geological Survey (USGS): Advanced Spaceborne Thermal Emission and Reflection Radiometer (ASTER) Level 1 Precision Terrain Corrected Registered At-Sensor Radiance Product (AST\_L1T): AST\_L1T Product User's Guide, 1, 1-68, doi: 10.3133/OFR20151171, 2015.